Supporting information

From Ashes to Riches: Microscale Phenomena Controlling Rare Earths Recovery from Coal Fly Ash

Sheila Gerardo,[a,b] *Artur R. Davletshin,*[a,b] *Staci L. Loewy,*[c] *Wen Song**[a,b,d]

[a] Hildebrand Department of Petroleum and Geosystems Engineering, The University of Texas at Austin, Austin, Texas 78712, United States

[b] Center for Subsurface Energy and the Environment, The University of Texas at Austin, Austin, Texas 78712, United States

[c] Department of Geological Sciences, The University of Texas at Austin, Austin, Texas 78712, United States

[d] Texas Materials Institute, The University of Texas at Austin, Austin, Texas 78712, United States

*Corresponding Author: Wen Song; Email: wensong@utexas.edu; Phone: (512) 471-5789.

Number of Pages: 17
Number of Figures: 8
Number of Tables: 4

Text S1-Acid Digestion and ICP-MS Analysis

Full Digestion for Initial Elemental Characterization. Approximately 35 mg of fly ash were dissolved overnight using a 1mL mixture of concentrated HF and HNO_3 at a 1:1 ratio. A mixture of HF and HNO_3 at a 4:1 volumetric ratio, respectively, was added to each beaker, and the digestion was carried out for three days. The samples were re-digested with 2 mL of HNO_3 overnight, followed by a 1 mL HCl digestion for three days. Beakers were ultrasonicated and the hydrochloric acid digestion was repeated until we achieved full dissolution. All digestions were carried at 160º C, and samples were dried in between digestion cycles. All resulting effluents were dried down and re-dissolved by adding 2 milliliters of 3 M HNO3. Appropriate dilutions were carried out, and trace elemental composition was determined via inductively coupled plasma mass spectrometry (Agilent 7500 ICP-MS). Initial digestion was run in triplicate.

Leaching Procedure. For the acid leaching experiments, samples were digested with 2 mL of full-strength aqua-regia for three days at 120º C. Following the acid digestion steps, samples were centrifuged, and leachates were transferred to clean beakers. All resulting effluents were dried down and re-dissolved by adding 2 milliliters of 3 M HNO3. Appropriate dilutions were carried out, and trace elemental composition was determined via inductively coupled plasma mass spectrometry (Agilent 7500 ICP-MS). Leaching experiments were run in triplicate.

ICP-MS Measurements. Major, minor, and trace elemental analyses were conducted using inductively coupled plasma mass spectrometry (ICP-MS, Agilent 7500) in solution mode. Effluents were diluted to less than 200 ppm of total dissolved solids for the trace elements analysis, and further diluted by a factor of 75 for the major and minor elemental analysis. Diluted aliquots were analyzed using three reaction cell modes: no gas mode, collision mode with helium, and

reaction mode with hydrogen. Rare earth elements were analyzed in collision mode with helium. Major elements were analyzed using all three modes; the final reported concentrations were selected based on the mode that yielded the most statistically robust measurements based on the quality control standards analyses.

Text S2- Microscale Imaging via SEM-EDS

Bulk Ash Imaging Settings. Spatial elemental characterization was conducted using a Scios 2 HiVac scanning electron microscope (SEM) equipped with an energy dispersive X-ray (EDX) detector and a backscattered electron detector (BSE). Visualization and EDX elemental mapping of the internal structure of fly ash were achieved at a voltage of 10 kV. At this operating voltage, the EDX depth of investigation was estimated to be ~0.6 microns based on Monte Carlo Simulations conducted using the Casino software. EDS linescan concentration profiles were obtained as duplicates, ~100 nm apart, and using a working voltage of 5 kV to reduce the volume of investigation.

PDMS Ash Imaging Settings. The PDMS-bound fly ash particulates were imaged before and after acid leaching using the Scios 2 HiVac SEM at a working voltage of 2-5 kV. EDS chemical data could not be properly collected due to charge accumulation resulting from the poor surface conductivity of the polymer.

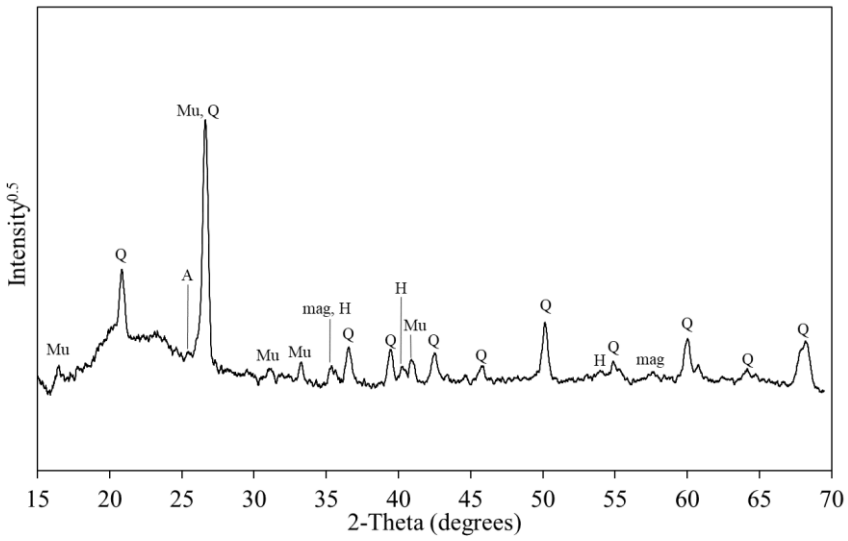

Figure S1. X-ray diffraction pattern of the ash sample. The major and minor phases include amorphous phase (identified by the hump in the low angle region), (Q) quartz, (Mu) mullite, (mag) magnetite, (H) hematite, and (A) anhydrite.

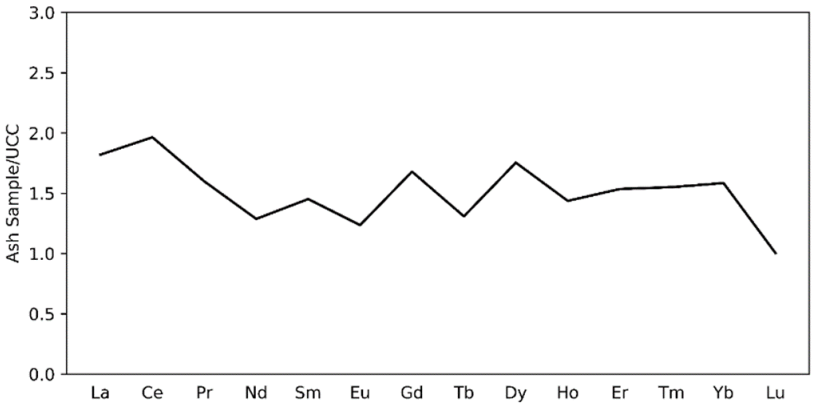

Figure S2. REEs total concentrations normalized with respect to the concentrations found in the Upper Continental Crust (UCC).

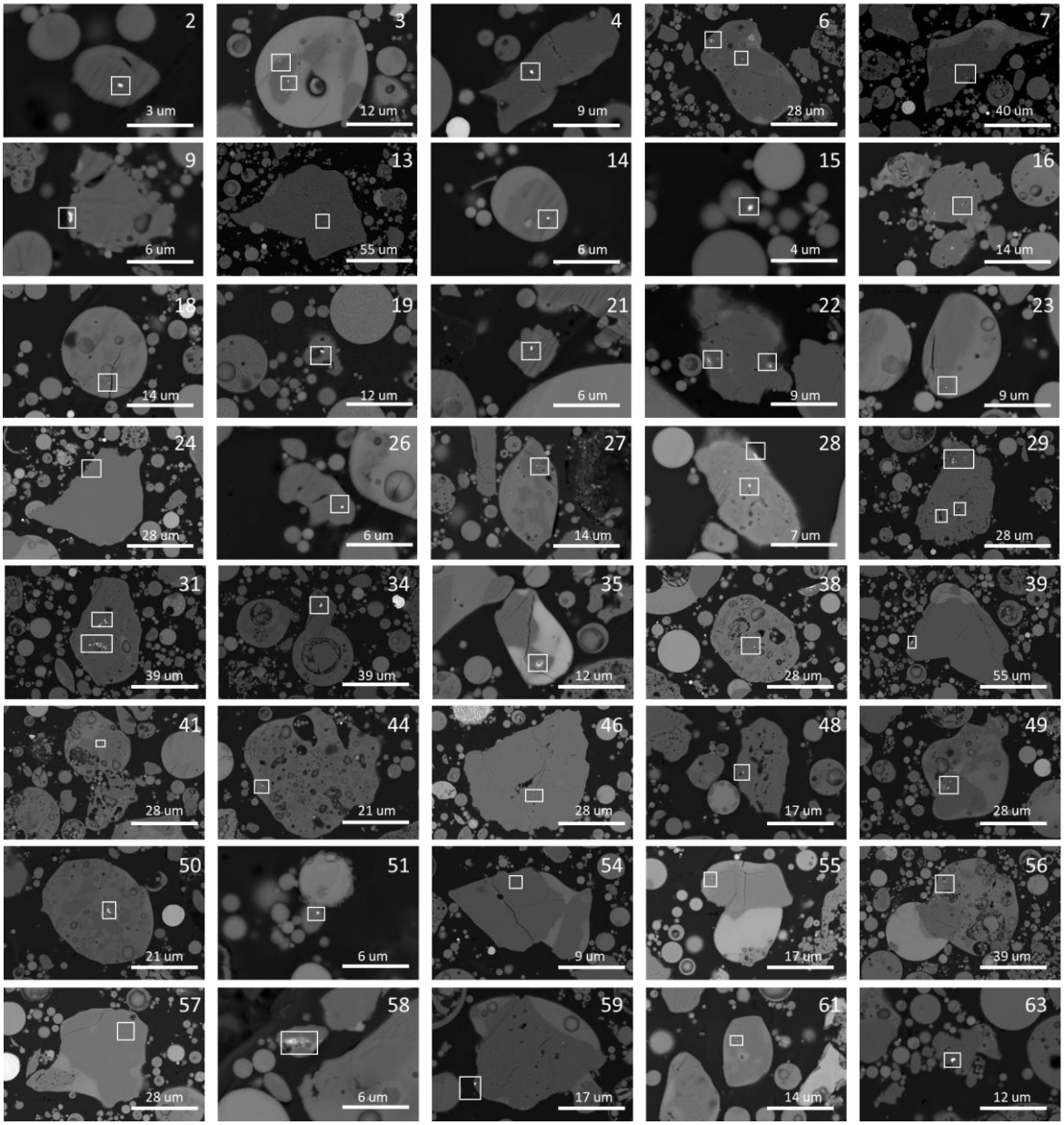

Figure S3. SEM images of the identified REEs present in dense particles. A total of 75 REEs minerals distributed across 40 dense aluminosilicate particles were analyzed in the initial characterization.

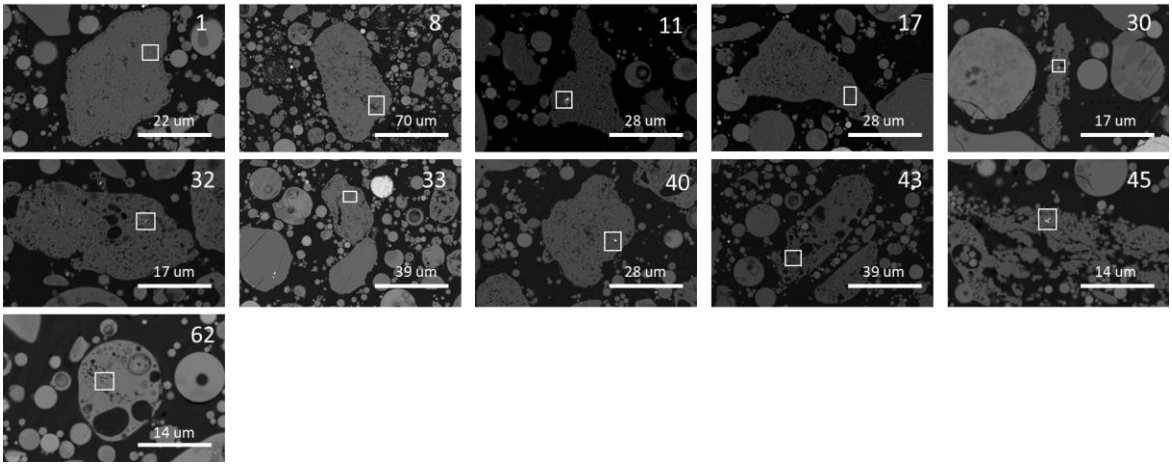

Figure S4. REEs minerals present in permeable particles. A total of 12 REEs minerals distributed across 11 permeable particles were identified and analyzed in the initial characterization.

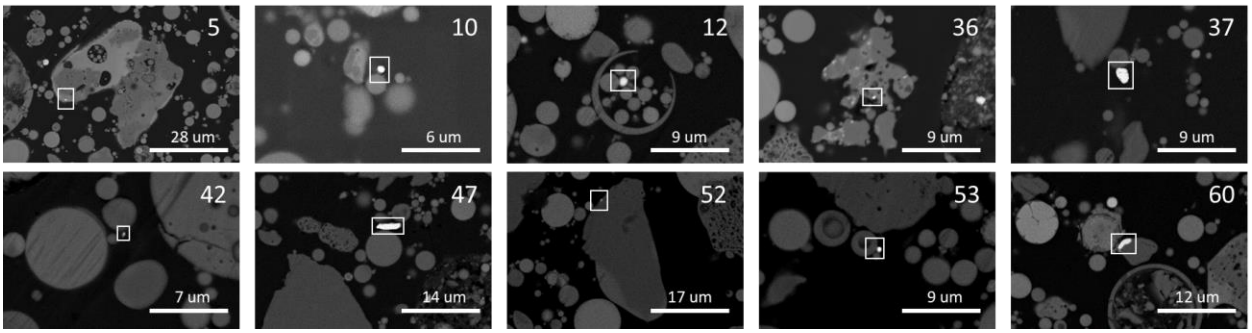

Figure S5. REEs minerals present as discrete particles, and at the surface of aluminosilicates. A total of 10 REEs minerals in this category were identified and analyzed in the initial characterization.

Table S1- Main elements identified in REE-bearing minerals shown in the figures S3-S5 obtained via EDS analysis.

Particle [a]	Elemental Composition of REE-bearing Minerals
1	Ce, Th, P
2	La, Ce, Nd, P
3	Ce, Nd, P
3.2	Ce, Nd, P
4	La, ,Ce, Nd, P
5	La, Ce, Nd, P
6	La, Ce, Nd, P
6.2	La, Ce, Nd, P
6.3	La, Ce, Nd, P
7	La, Ce, P
8	Ce, P
9	Y, Si, Zr
10	La, Ce, Nd, P
12	La, Ce, Nd, O
13	La, Ce, Nd, P
14	La, Ce, P
15	La, Ce, Nd, P
16	Ce, Nd, P
17	Ce, Nd, Th, P
18	La, Ce, Nd, P
19	La, Ce, Nd, P
21	La, Ce, Nd, P
22	La, Ce, Nd, P
22.2	La, Ce, Nd, P
24	La, Ce, P
25	La, Ce, Pr, P
26	Ce, Nd, P
27	Ce, Nd, P
28	Ce, P
28.2	La, Ce, P
29	La, Ce, Nd, P
29.2	La, Ce, Nd, P
29.3	La, Ce, Nd, P
29.4	La, Ce, Nd, P
29.5	La, Ce, Nd, P
29.6	La, Ce, Nd, P

29.7	La, Ce, Nd, P
29.8	La, Ce, Nd, P
29.9	La, Ce, Nd, P
29.10	La, Ce, Nd, P
29.11	La, Ce, Nd, P
29.12	La, Ce, Nd, P
30	Ce, Nd, Th, P
31	La, Ce, Nd, P
31.2	La, Ce, Nd, P
31.3	La, Ce, Nd, P
31.4	La, Ce, Nd, P
31.5	La, Ce, Nd, P
31.6	La, Ce, Nd, P
31.7	La, Ce, Nd, P
31.8	La, Ce, Nd, P
31.9	La, Ce, Nd, P
31.10	La, Ce, Nd, P
31.11	La, Ce, Nd, P
31.12	La, Ce, Nd, P
31.13	La, Ce, Nd, P
31.14	La, Ce, Nd, P
31.15	La, Ce, Nd, P
31.16	La, Ce, Nd, P
32	Ce, Nd, P
33	Ce, Th, P
34	La, Ce, Nd, P
35	La, Ce, Nd, P
36	Y, Si, Zr
37	La, Ce, Pr, Nd, P
38	La, Ce, Nd, P
39	La, Ce, Nd, P
40	Ce, Nd, P
41	La, Ce, Pr, P
42	Ce, P
43	La, Nd, P
44	La, Ce, Nd, P
45	Ce, P
45.2	Ce, P
46	Ce, Nd, P
47	La, Ce, Nd, Th, P
48	Ce, Nd, P
49	La, Ce, Nd, Pr, P
49.2	La, Ce, Nd, Pr, P

50	La, Ce, Nd, P
51	La, Ce, Nd, P
52	La, Ce, P
53	La, Ce, Nd, O
54	Ce, Nd, P
55	Ce, P
56	La, Ce, Nd, P
57	La, Ce, P
58	La, Ce, Nd, P
58.2	La, Ce, Nd, P
58.3	La, Ce, Nd, P
59	Ce, P
60	Y, Si, Zr
61	Nd, P
62	Ce, Nd, Th, P
62.2	Ce, Nd, Th, P
63	La, Ce, Nd, Th, P

[a] Particle numbers with decimals are used to denote different REEs minerals within the same particle.

Table S2- Classification, and composition (obtained via EDS mapping and averaged across the representative elemental volume) of the matrix surrounding REEs shown in the figures S3-S5, imaged during the initial characterization.

Particle [a]	classification	Si (wt%)	Al (wt%)	Ca (wt%)	Na (wt%)	Mg (wt%)	Fe (wt%)	K (wt%)
1	permeable	22.8	22.5	0.8	0.0	0.6	3.7	0.1
2	dense	38.5	0.7	0.6	0.6	0.5	7.7	0.0
3.1	dense	37.7	1.7	1.9	0.7	0.6	4.5	0.3
3.2	dense	38.6	0.4	0.8	0.7	0.3	4.1	1.1
4	dense	38.5	0.7	0.4	0.4	0.4	5.6	0.0
5	surface-bound	-	-	-	-	-	-	-
6.1	dense	35.1	1.0	0.4	1.2	0.4	8.8	0.0
6.2	dense	34.7	0.9	0.2	1.2	0.3	8.8	0.0
6.3	dense	38.3	1.2	0.3	0.2	0.4	7.8	0.0
7	dense	40.8	0.2	0.1	0.7	0.3	4.3	0.0
8	permeable	21.8	20.1	0.3	0.4	0.4	4.7	0.7
9	dense	25.5	1.7	1.2	1.1	1.0	7.4	0.0
10	discrete	-	-	-	-	-	-	-
12	discrete	-	-	-	-	-	-	-
13	dense	41.5	1.2	0.6	0.9	0.4	5.0	0.0
14	dense	37.3	1.0	0.1	0.7	0.7	0.0	1.0
15	dense	27.0	2.2	0.8	0.9	0.7	9.7	1.1
16	dense	37.8	1.5	0.3	0.6	0.7	7.2	0.7
17	permeable	20.6	21.7	1.1	0.6	0.9	6.5	0.0
18	dense	36.3	3.0	0.7	1.7	0.6	8.2	1.4
19	dense	28.2	12.6	0.0	2.0	1.2	0.0	0.0
21	dense	38.9	1.0	0.7	0.6	0.5	6.9	0.0
22.1	dense	31.3	4.6	1.5	1.7	0.8	6.4	1.7
22.2	dense	34.0	4.9	1.1	1.4	0.9	5.8	1.6
23	dense	38.6	3.6	1.0	1.0	1.1	6.6	0.2
24	dense	30.7	0.3	0.0	0.0	0.2	1.6	0.0
26	dense	41.0	0.4	0.3	0.5	0.5	5.7	0.0
27	dense	37.9	2.3	0.9	0.6	0.6	5.1	0.0
28.1	dense	24.3	2.5	1.3	1.7	0.4	0.0	0.0
28.2	dense	38.4	1.4	1.0	0.4	0.4	0.0	0.0
29.1	dense	41.8	0.9	0.9	0.4	0.7	0.0	0.0
29.2	dense	45.0	1.7	0.4	1.0	0.4	0.0	0.0
29.3	dense	38.1	0.4	0.5	1.3	0.8	0.0	0.0
29.4	dense	36.2	1.2	0.4	1.2	0.7	0.0	0.0

29.5	dense	38.2	0.7	0.5	1.1	0.6	0.0	0.0
29.6	dense	40.7	0.7	0.8	1.2	0.9	0.0	0.0
29.7	dense	38.6	0.0	0.1	0.5	0.4	0.0	0.0
29.8	dense	41.2	0.4	0.6	0.8	0.5	0.0	0.0
29.9	dense	39.8	0.7	1.0	0.5	0.5	0.0	0.0
29.10	dense	38.9	0.5	0.8	0.7	0.3	0.0	0.0
29.11	dense	42.1	0.8	1.8	0.5	0.3	0.0	0.0
29.12	dense	41.2	1.3	0.5	0.7	0.5	0.0	0.0
30	permeable	25.7	18.7	0.0	0.8	0.7	4.6	1.0
31.1	dense	40.4	2.1	0.7	0.7	0.8	1.9	2.2
31.2	dense	39.2	1.6	0.8	1.1	0.6	4.4	1.8
31.3	dense	37.3	4.5	0.2	1.9	1.4	9.8	2.9
31.4	dense	39.8	2.4	0.2	0.6	1.0	10.3	0.9
31.5	dense	37.3	2.0	0.0	1.0	0.6	6.8	0.6
31.6	dense	38.8	0.6	1.5	1.2	1.2	5.0	1.3
31.7	dense	29.1	5.0	2.9	1.7	0.3	8.9	1.3
31.8	dense	33.3	3.6	1.1	2.1	0.8	8.3	1.7
31.9	dense	34.5	6.9	2.5	1.6	0.7	6.9	2.7
31.10	dense	34.0	4.5	1.1	1.7	1.2	5.6	2.0
31.11	dense	35.8	4.5	1.3	1.6	1.6	9.2	0.0
31.12	dense	38.9	2.2	0.2	0.6	0.6	10.8	0.3
31.13	dense	35.2	4.0	1.1	2.3	1.3	5.7	0.9
31.14	dense	38.2	4.5	1.0	1.3	0.5	5.4	1.6
31.15	dense	38.9	1.8	1.5	1.1	1.0	3.9	0.0
31.16	dense	37.6	1.6	0.3	0.6	0.5	8.0	1.3
32	permeable	23.5	15.5	2.1	0.6	0.6	0.0	0.0
33	permeable	20.5	22.7	0.3	2.0	0.9	6.8	0.7
34	dense	38.0	0.7	1.4	0.6	0.2	5.4	0.5
35	dense	29.8	4.4	1.1	1.3	0.9	15.2	2.0
36	surface-bound	-	-	-	-	-	-	-
37	discrete	-	-	-	-	-	-	-
38	dense	37.5	1.3	0.2	1.1	0.7	4.3	1.5
39	dense	28.0	0.8	2.0	1.2	0.7	4.9	0.0
40	permeable	21.4	21.9	1.0	1.3	0.8	5.2	0.8
41	dense	40.3	1.3	0.8	1.1	0.4	8.4	0.5
42	discrete	-	-	-	-	-	-	-
43	permeable	22.6	23.1	1.2	0.9	1.0	3.4	0.6
44	dense	29.7	7.6	1.1	1.7	2.5	7.4	2.8
45.1	permeable	22.8	22.6	1.1	1.0	0.9	0.0	0.5
45.2	permeable	24.4	21.8	1.6	1.1	0.8	0.0	0.1
46	dense	39.6	0.6	0.7	1.2	0.4	0.0	1.1

47	discrete	-	-	-	-	-	-	-
48	dense	43.0	1.0	0.0	0.6	0.8	5.2	0.6
49.1	dense	35.4	0.9	1.6	1.2	0.9	6.8	0.5
49.2	dense	33.4	2.3	1.0	1.3	0.9	5.9	0.9
50	dense	32.2	2.1	1.5	0.9	0.8	8.7	2.0
51	dense	32.5	1.8	0.9	1.3	1.8	4.3	1.2
52	surface-bound	-	-	-	-	-	-	-
53	discrete	-	-	-	-	-	-	-
54	dense	40.9	0.7	0.3	0.8	0.5	5.0	0.7
55	dense	39.7	1.2	1.6	1.2	0.5	4.5	1.7
56	dense	27.9	7.0	1.8	0.6	0.6	7.4	1.5
57	dense	40.7	0.8	0.6	0.7	0.3	2.1	0.0
58.1	dense	23.0	9.9	2.8	1.3	1.8	0.0	0.5
58.2	dense	27.1	7.9	6.2	1.2	2.1	0.0	1.3
58.3	dense	28.3	4.6	6.6	0.8	2.5	0.0	0.5
59	dense	26.0	0.5	2.1	0.9	1.2	5.7	0.6
60	surface-bound	-	-	-	-	-	-	-
61	dense	37.3	0.7	0.0	1.1	0.8	5.5	1.5
62.1	permeable	19.0	21.8	0.5	1.4	0.6	5.1	0.0
62.2	permeable	18.8	21.8	0.5	1.3	0.6	5.5	0.0
63	dense	30.9	2.0	1.6	1.0	1.0	7.2	1.5

[a] Particle numbers with decimals are used to denote different REEs minerals within the same particle.

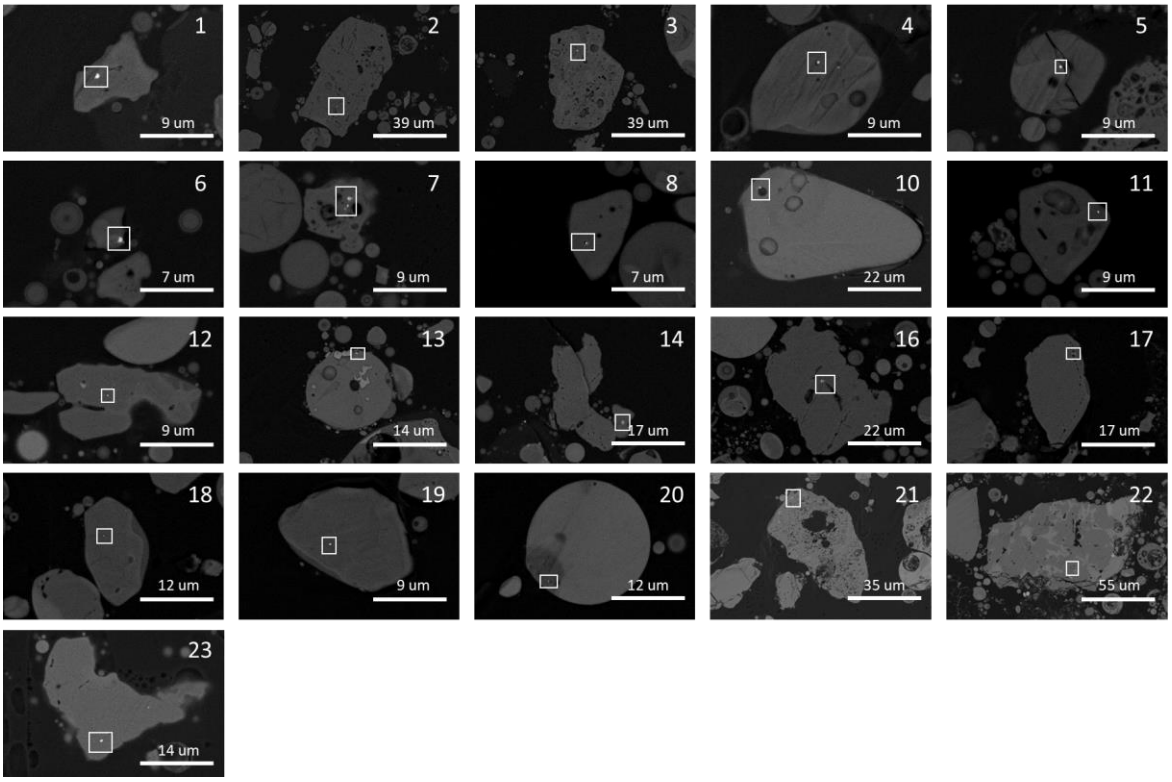

Figure S6. SEM images of REEs minerals identified in the solid residue after acid leaching.

Table S3- Classification, and composition (obtained via EDS mapping and averaged across the representative elemental volume) of the REEs-hosting phases shown in the figure S6, imaged after leaching.

Particle [a]	classification	Si (wt%)	Al (wt%)	Ca (wt%)	Na (wt%)	Mg (wt%)	K (wt%)
1	dense	36.4	1.0	0.6	1.1	0.6	0.5
2	dense	40.3	2.0	0.0	0.3	1.0	2.1
3	dense	38.2	2.7	0.2	1.5	0.6	4.7
4	dense	41.6	0.8	0.0	0.8	0.3	0.5
5	dense	35.3	1.8	1.2	1.4	1.2	2.1
6	dense	24.8	2.8	0.0	0.9	1.7	1.7
7.1	dense	37.9	0.8	0.0	1.6	0.6	0.7
7.2	dense	44.6	1.3	0.0	0.9	0.3	1.1
7.3	dense	40.5	1.4	0.0	0.7	0.4	0.6
8	dense	46.1	0.9	0.0	0.0	0.0	0.0
10	dense	30.0	9.5	0.0	2.3	0.0	0.0
11	dense	33.3	1.4	0.0	1.0	0.5	0.0
12	dense	40.9	0.4	0.3	1.0	0.3	0.1
13	dense	22.8	6.8	0.0	4.9	0.7	4.8
14	dense	35.2	1.3	0.0	1.1	0.0	0.0
16.1	dense	43.6	1.8	0.9	0.6	0.5	0.0
16.2	dense	42.5	1.8	0.9	0.9	0.5	0.0
17.1	dense	43.0	1.0	0.0	0.6	0.0	0.1
17.2	dense	41.9	1.5	0.0	1.0	0.0	0.3
18	dense	42.1	0.9	1.1	0.5	0.4	1.3
19	dense	42.0	0.8	0.0	0.9	0.9	0.7
20	dense	38.4	1.2	1.6	0.9	0.5	0.8
21	permeable	27.0	12.8	3.5	1.8	0.2	0.0
22	dense	38.5	3.8	0.0	0.0	0.2	2.1
23	dense	44.3	0.7	0.0	0.0	0.0	0.5

[a] Particle numbers with decimals are used to denote different REEs minerals within the same particle.

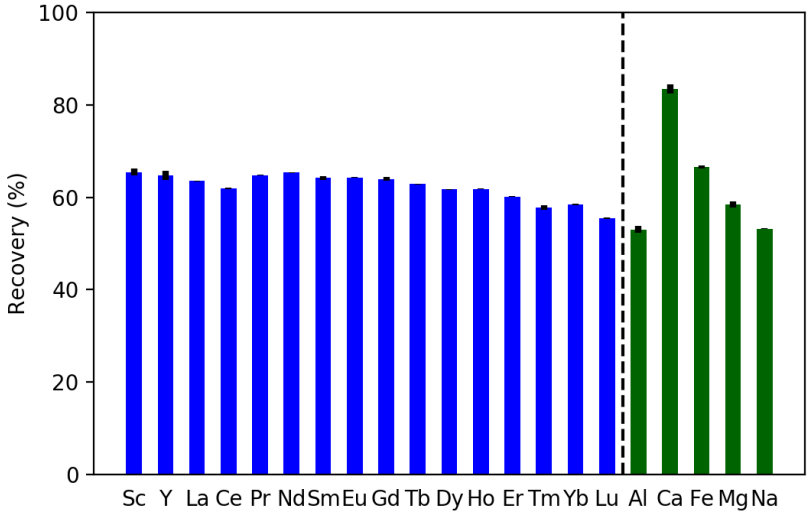

Figure S7. Elemental recovery efficiencies of REEs (in blue), and major metals (in green) based on leachates analysis using ICP-MS. Slight preferential recovery of lighter REEs is observed. Large variations among major metals recovery are a result of the different bulk mineral phases in the initial ash.

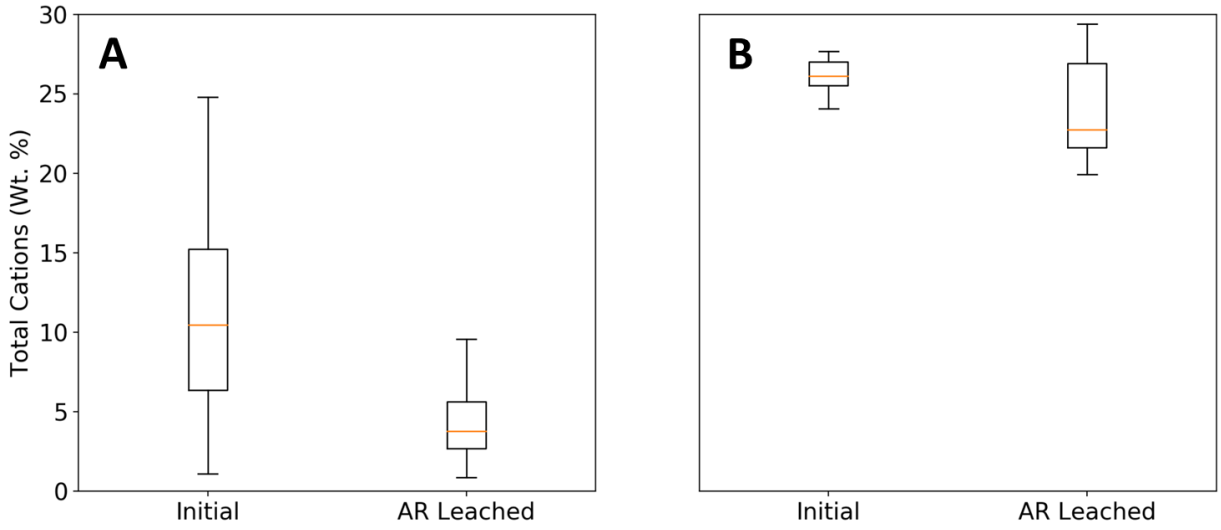

Figure S8. Metal concentrations (Al, Na, Ca, Mg, K, Fe) measured in (A) REEs-hosting dense particles indicate that REEs minerals embedded in metal-rich particles were recovered during AR leaching, leaving only the REEs present in particles low metal content. For (B) permeable particles, there are no significant differences in metal content before and after leaching. Due to a limited number of REEs-hosting permeable particles imaged after leaching, (B) compares overall changes in permeable particles and is not limited to REEs-hosting particles.

Table S4- The Mann-Whitney U test computed using the DataTab software shows that statistical differences exist between the composition of dense particles before and after leaching, whereas permeable particles pre- and post-leaching show statistically similar metal content.

	dense particles (initial vs leached)	permeable particles (initial vs leached)
U	352	30
p-value	<0.001	0.574